



1 A new bed elevation model for the Weddell Sea sector of the West 2 Antarctic Ice Sheet

3
4 Hafeez Jeofry^{1,2}, Neil Ross³, Hugh F.J. Corr⁴, Jilu Li⁵, Prasad Gogineni⁶ and Martin J. Siegert¹

5 ¹Grantham Institute and Department of Earth Science and Engineering, Imperial College London,
6 South Kensington, London, UK

7 ²School of Marine Science and Environment, Universiti Malaysia Terengganu, Kuala Terengganu,
8 Terengganu, Malaysia

9 ³School of Geography, Politics and Sociology, Newcastle University, Claremont Road, Newcastle
10 Upon Tyne, UK

11 ⁴British Antarctic Survey, Natural Environment Research Council, Cambridge, UK

12 ⁵Center for the Remote Sensing of Ice Sheets, University of Kansas, Lawrence, Kansas, USA

13 ⁶ECE Department, The University of Alabama, Tuscaloosa, AL 35487, USA

14

15 *Correspondence to:* Hafeez Jeofry (h.jeofry15@imperial.ac.uk)

16

17 **Abstract.** We present a new bed elevation digital elevation model (DEM), with a 1 km spatial resolution, for the Weddell Sea
18 sector of the West Antarctic Ice Sheet. The DEM has a total area of ~125,000 km² covering the Institute, Möller and Foundation
19 ice streams and the Bungenstock ice rise. In comparison with the Bedmap2 product, our DEM includes several new
20 aerogeophysical datasets acquired by the Center for Remote Sensing of Ice Sheets (CReSIS) through the NASA Operation
21 IceBridge (OIB) program in 2012, 2014 and 2016. We also update bed elevation information from the single largest existing
22 dataset in the region, collected by the British Antarctic Survey (BAS) Polarimetric Airborne Survey Instrument (PASIN) in
23 2010-11, as BEDMAP2 included only relatively crude ice thickness measurements determined in the field for quality control
24 purposes. This has resulted in the deep parts of the topography not being visible in the fieldwork non-SAR processed
25 radargrams. While the gross form of the new DEM is similar to Bedmap2, there are some notable differences. For example,
26 the position and size of a deep trough (~2 km below sea level) between the ice sheet interior and the grounding line of
27 Foundation ice stream has been redefined. From the revised DEM, we are able to better derive the expected routing of basal
28 water at the ice-bed interface, and by comparison with that calculated using Bedmap2 we are able to assess regions where
29 hydraulic flow is sensitive to change. Given the sensitivity of this sector of the ice sheet to ocean-induced melting at the
30 grounding line, especially in light of improved definition of the Foundation ice stream trough, our revised DEM will be of
31 value to ice-sheet modelling in efforts to quantify future glaciological changes in the region, and therefore the potential impact
32 on global sea level. The new 1 km bed elevation product of the Weddell Sea sector, West Antarctica can be found in the
33 <http://doi.org/10.5281/zenodo.1035488>.
34

35 1. Introduction

36

37 The Intergovernmental Panel on Climate Change (IPCC) projected that global sea level could increase by between 0.26 and
38 0.82 m by the end of the 21st century (Stocker, 2014). The rising oceans pose a threat to the socio-economic activities of
39 hundreds of millions of people, mostly in Asia, living at and close to the coastal environment. Several processes drive sea level
40 rise (e.g. thermal expansion of the oceans), but the largest potential factor comes from the ice sheets in Antarctica. The West
41 Antarctic Ice Sheet (WAIS), which if melted would raise sea-level by around 3.5 m, is grounded on a bed which is ~2 km
42 below sea level (Bamber et al., 2009b; Ross et al., 2012; Fretwell et al., 2013) allowing the ice margin to have direct contact
43 with ocean water. One of the most sensitive regions of the WAIS to potential future ocean warming is the Weddell Sea (WS)
44 sector (Ross et al., 2012; Wright et al., 2014). Ocean modelling studies project that changes in present ocean circulation could
45 bring warm ocean water into direct contact with the grounding lines at the base of the Filchner Ronne Ice Shelf (FRIS) (Hellmer
46 et al., 2012; Wright et al., 2014; Martin et al., 2015; Ritz et al., 2015; Thoma et al., 2015), which would act in a similar manner
47 to the ocean-induced basal melting under the Pine Island Glacier ice shelf (Jacobs et al., 2011). Enhanced melting of the FRIS
48 could lead to a decrease in the buttressing support to the upstream grounded ice, encouraging enhanced flow from the parent
49 ice mass to the ocean (Jacobs et al., 2011). A recent modelling study, using a general ocean circulation model coupled together
50 with a 3D thermodynamic ice sheet model, simulated the inflow of warm ocean water into the Ronne-Filchner ice shelf cavity
51 on a 1000 year timescale (Thoma et al., 2015). A second modelling study, this time using an ice sheet model, indicated that
52 the Institute and Möller ice streams are highly sensitive to melting at the grounding lines; with grounding line retreat up to 180
53 km possible across the Institute and Möller ice streams (Wright et al., 2014). While the Foundation ice stream was shown to



54 be relatively resistant to ocean-induced change (Wright et al., 2014), a dearth of geophysical measurements of ice thickness
55 across the ice stream at the time means the result may be inaccurate.

56 Recently, investigations of ice-sheet change have been regarded as a scientific priority for the next two decades and
57 beyond (Kennicutt et al., 2014; Kennicutt et al., 2016). While satellite images can provide evidence of surface elevation
58 changes, they are unable to provide information on the subglacial environment and, hence, are limited in their ability to uncover
59 ice-sheet flow processes and their change.

60 The primary tool for measurements of subglacial topography and basal ice-sheet conditions is radio-echo sounding (RES)
61 (Dowdeswell and Evans, 2004; Bingham and Siegert, 2007). The first topographic representation of the land surface beneath
62 the entire Antarctic ice sheet (Drewry, 1983) was published by the Scott Polar Research Institute, University of Cambridge,
63 (SPRI) in collaboration with the US National Science Foundation Division of Polar Programmes (NSF-DPP) and the Technical
64 University of Denmark (TUD), following multiple field seasons of RES surveying in the 1970s (Drewry and Meldrum, 1978;
65 Drewry et al., 1980; Jankowski and Drewry, 1981; Drewry, 1983). The compilation (Drewry, 1983) included folio maps of
66 bed topography and ice-sheet surface elevation and thickness. The bed was digitized on a 20 km grid for use in ice-sheet
67 modelling (Budd et al., 1984). However, only around one third of the continent was measured at a line spacing of less than
68 ~100 km (Lythe and Vaughan, 2001), making the elevation product highly erroneous in many places, with obvious knock-on
69 consequences for modelling. Several RES campaigns were thenceforth conducted, and the data from them were compiled into
70 a single new Antarctic bed elevation product, named Bedmap (Lythe and Vaughan, 2001). The Bedmap DEM had a cell
71 resolution of 5 km, and included over 1.4 million km and 250,000 km line track of airborne and ground-based radio-echo
72 sounding data, respectively. Subglacial topography was extended north to 60°S, for purposes of ice sheet modelling, and
73 determination of ice-ocean interactions. Since its release, Bedmap has proved to be highly useful for a wide range of research,
74 yet inherent errors within it (e.g. inaccuracies in the DEM and conflicting grounding line representation with observations)
75 limited its effectiveness to the community (Le Brocq et al., 2010; Fretwell et al., 2013). After 2001, several new RES surveys
76 were conducted, to fill data gaps revealed by Bedmap, especially during and after the 4th International Polar Year (2007-9).
77 These new data led to the most recent Antarctic bed project, named Bedmap2 (Fretwell et al., 2013). Despite significant
78 improvements in the resolution and accuracy of Bedmap2 compared with Bedmap, a number of inaccuracies and poorly
79 sampled areas persist where only 34% of cells have data and 80% have data within the range of 20 km (Fretwell et al., 2013;
80 Pritchard, 2014), preventing a comprehensive appreciation of the complex relation between the topography and internal ice-
81 sheet processes, and indeed a full appreciation of the sensitivity of the Antarctic ice sheet to ocean and atmospheric warming.

82 The Weddell Sea sector of the WAIS was the subject of a major aerogeophysical survey in 2010-11 (Ross et al., 2012),
83 revealing the ~2 km deep Robin Subglacial Basin immediately upstream of present-day grounding lines, from which
84 confirmation of the ice-sheet sensitivity from ice-sheet modelling was determined (Wright et al., 2014). Further geophysical
85 surveying of the region has been undertaken since Bedmap2 (Siegert et al., 2016b), improving knowledge of the land surface
86 beneath the ice sheet. This has provided an enhanced appreciation of the importance of basal hydrology to ice flow (Siegert et
87 al., 2016b), and the complexities of the interaction of basal water flow, bed topography and ice surface elevation, emphasising
88 the importance of developing accurate and high resolution DEMs (Lindbäck et al., 2014; Siegert et al., 2014; Graham et al.,
89 2016).

90 In this paper, we present a revised bed DEM for the Weddell Sea sector, based on a compilation of airborne radar surveys.
91 The DEM has a total area of ~125,000 km² and a grid cell resolution of 1 km. From this dataset, we reveal the expected
92 pathways of subglacial water, and discuss the differences between the new DEM and Bedmap2.

94 2. Study area

95
96 The study area is located in the Weddell Sea sector of WAIS covering the Institute, Möller and Foundation ice streams, and
97 the Bungenstock ice rise (Fig. 1). The DEM extends 135 km grid south of the Bungenstock ice rise, 195 km grid east of the
98 Foundation ice stream, over the Pensacola Mountain and 185 km grid west of the Institute ice stream. In comparison with the
99 Bedmap2, our new DEM benefits from several new airborne geophysical datasets (e.g. NASA OIB 2012, 2014 and 2016). In
100 addition, the new DEM is improved by the inclusion of ice thickness picks derived from SAR-processed RES data from the
101 BAS aerogeophysical survey of the Institute and Möller ice streams conducted in 2010/2011. This has improved the accuracy
102 of the determination of the ice bed interface in comparison to Bedmap2. The data and methods used in this study are mostly
103 similar to Jeofry et al. (2017), however, we have expanded the boundaries of our new bed elevation DEM by focussing across
104 the Weddell Sea sector relative to the Institute ice stream as the main focus in Jeofry et al. (2017). In addition, this paper
105 focuses on discussing the geomorphology and improvement that have been made between our new bed elevation DEM and
106 Bedmap2 product whereas Jeofry et al. (2017) discuss on the hitherto unknown subglacial embayment and its effect to the ice-
107 sheet dynamics.

109 3. Data and methods



110 The radio echo sounding (RES) data used in this study were compiled from four main sources (Fig. 1a). First, SPRI data
111 collected during six survey campaigns between 1969 and 1979 (Drewry, 1983). Second, the BAS airborne radar survey
112 accomplished during the austral summer 2006/07 (GRADES/IMAGE) (Ashmore et al., 2014). Third, the BAS survey of the
113 Institute and Möller ice streams, undertaken in 2010/2011 (IMAFI) (Ross et al., 2012). Finally, flights conducted by the Center
114 for the Remote Sensing of Ice Sheet (CReSIS) during the NASA OIB programme in 2012, 2014 and 2016 (Gogineni, 2012)
115 supplement the data previously used in the Bedmap2 bed elevation product to accurately characterize the subglacial topography
116 of this part of the Weddell Sea sector.

117

118 3.1 Scott Polar Research Institute survey

119

120 The SPRI surveys of the 1970s covered a total area of 6.96 million km² (~40% of continental area) across West and East
121 Antarctica (Drewry et al., 1980). The data were collected using a pulsed radar system operating at centre frequencies of 60 and
122 300 MHz (Christensen, 1970; Skou and Søndergaard, 1976) equipped on NSF C-130R Hercules aircraft (Drewry and
123 Meldrum, 1978; Drewry et al., 1980; Jankowski and Drewry, 1981; Drewry, 1983). The 60 MHz antennas, built by the
124 Technical University of Denmark, comprised an array of four half wave dipoles which were mounted in neutral aerofoil
125 architecture of insulating components beneath the starboard wing. The 300 MHz antennas were composed of four dipoles
126 attached underneath a reflector panel below the port wing. The purpose of this unique design was to improve the backscatter
127 acquisition and directivity. The returned signals were archived on 35 mm film and dry-silver paper by a fibre optic oscillograph.
128 Aircraft navigation was assisted using an LTN-51 inertial navigation system giving a positional error of around 3 km.
129 Navigation and other flight data were stored on magnetic and analogue tape by an Airborne Research Data System (ARDS)
130 constructed by US Naval Weapons Center. The system recorded up to 100 channels of six-digit data with a sampling rate of
131 303 Hz per channel. Navigation, ice thickness and ice surface elevation records were recorded every 20 seconds, corresponding
132 to around 1.6 km between each data point included on the Bedmap2 product. The data was initially recorded on a 35-mm
133 photographic film (i.e. Z-scope radargrams) and was later scanned and digitized, as part of a NERC Centre for Polar
134 Observation and Modelling (CPOM), in 2004. Each film records were scanned separately and reformatted to form a single
135 electronic image of a RES transect. The scanned image was loaded into an image analysis package (i.e. ERDAS Imagine) to
136 trace the internal layers which were then digitized. The dataset was later standardized with respect to the ice surface.

137

138 3.2 BAS GRADES/IMAGE surveys

139

140 The GRADES/IMAGE project was conducted during the austral summer of 2006/2007 and consisted of ~27,550 km of RES
141 data flown across the Antarctic Peninsula, Ellsworth Mountain and Filchner-Ronne ice shelf. The BAS Polarimetric radar
142 Airborne Science Instrument (PASIN) radar operates at a centre frequency of 150 MHz, has a 10 MHz bandwidth and a pulse-
143 coded waveform acquisition rate of 312.5 Hz (Corr et al., 2007; Ashmore et al., 2014). The PASIN system interleaves a pulse
144 and CHIRP signal to acquire two datasets simultaneously. Pulse data is used for imaging layering in the upper half of the ice
145 column, whilst the more powerful CHIRP is used for imaging the deep-ice and sounding the ice sheet bed. The peak transmitted
146 power of the system is 4 kW. The spatial sampling interval of ~20 m resulted in ~50,000 traces of data for a typical 4.5-hour
147 flight. The radar system consisted of 8 folded dipole elements; 4 transmitters on the port side and 4 receivers on the starboard
148 side. The receiving “backscatter” signal was digitized and sampled using a sub-Nyquist sampling technique and are then
149 recorded on magnetic tape drives. The pulses are compressed using a matched filter, and sidelobes are minimized using a
150 Blackman window. Aircraft position was recorded by an onboard carrier wave global positioning system (GPS). The absolute
151 positional accuracy for GRADES/IMAGE was 0.1 m (Corr et al., 2007). Synthetic Aperture Radar (SAR) processing was not
152 applied to the GRADES/IMAGE data.

153

154 3.3 BAS Institute-Möller Antarctic Funding Initiative surveys

155

156 The BAS data acquired during the IMAFI project consist of ~25,000 km of aerogeophysical data collected during 27 flights
157 from two field camps. 17 flights were flown from C110 (-82° 37' 30"N, 280° 59' 13.2"E), and the remaining 10 flights were
158 flown from Patriot Hills (-80° 19' 60"N, 278° 34' 60"E) (Fig. 1b). Data were acquired with the same PASIN radar used for the
159 GRADES/IMAGE survey. The data rate of 13 Hz gave a spatial sampling interval of ~10 m for IMAFI. The system was
160 installed on the BAS de Havilland Twin Otter aircraft with a four-element folded dipole array mounted below the starboard
161 wing used for reception and the identical array attached below the port wing for transmission. The flights were flown in a
162 stepped pattern during the IMAFI survey to optimise potential field data (gravity and magnetics) acquisition (Fig. 1a). Leica
163 500 and Novatel DL-V3 GPS receivers were installed in the aircraft, corrected with two Leica 500 GPS base stations which
164 were operated throughout the survey to calculate the position of the aircraft (Jordan et al., 2013). The positional data were
165 referenced to the WGS 84 ellipsoid. The absolute positional accuracy for IMAFI (the standard deviation for the GPS positional



166 error) was calculated to be at 7 cm and 20 cm in the horizontal and vertical dimensions (Jordan et al., 2013). 2-D focused SAR
167 processing (Hélière et al., 2007) (see section 4.1) was applied to the IMAFI data.

168

169 3.4 NASA OIB / CReSIS surveys

170

171 The OIB project surveyed a total distance of ~32,693 km, ~52460 km and ~53672 km in Antarctica in 2012, 2014 and 2016,
172 respectively, using the Multichannel Coherent Radar Depth Sounder (MCoRDS) system developed at the University of Kansas
173 (Gogineni, 2012). The system was operated with a carrier frequency of 195 MHz, a bandwidth of 10 MHz and 50 MHz in
174 2012 (Rodríguez-Morales et al., 2014) and 2014 onwards (Siegert et al., 2016b). The radar consisted of a five – element
175 antenna array housed in a customized antenna fairing which is attached beneath the NASA DC – 8 aircraft fuselage (Rodríguez-
176 Morales et al., 2014). The five antennas were operated from a multichannel digital direct synthesis (DDS) controlled waveform
177 generator enabling the user to adjust the frequency, timing, amplitude and phase of each transmitted waveform (Shi et al.,
178 2010). The radar employs an eight-channel waveform generator to emit eight independent transmit chirp pulses. The system
179 is capable of supporting 5 receiver channels with Analog Devices AD9640 14 bit analog-to-digital converter (ADC) acquiring
180 the waveform at a rate of 111 MHz in 2012 (Gogineni, 2012). The system was upgraded in 2014 and 2016 utilizing six channel
181 chirp generation and supports six receiver channels with a waveform acquisition rate at 150 MHz. Multiple receivers allow
182 array processing to suppress surface clutter in the cross track direction which could potentially conceal weak echoes from the
183 ice – bed interface (Rodríguez-Morales et al., 2014). The radar data are synchronized with the GPS and inertial navigation
184 system (INS) using the GPS time stamp to determine the location of data acquisition.

185

186 4. Data processing

187

188 Airborne RES assumes the radar pulse propagates through ice at a constant wave speed of 0.168 m ns^{-1} , since glacial ice is
189 assumed to be homogenous (Lythe and Vaughan, 2001). The radar pulse travels through a medium until it meets a boundary
190 of differing dielectric constant, which causes some of the radio wave to be reflected and subsequently captured by the receiver
191 antenna. There are three factors causing dielectric contrast in ice sheets; density variations in the upper 700 m, acidic layers
192 caused by the aerosol from volcanic activity, and ice permittivity variations from crystal fabrics (Siegert, 1999; Corr et al.,
193 2007). The time travelled by the radar pulse between the upper and lower reflecting surface is measured and converted to ice
194 thickness with reference to WGS 84 (Fig. 2). The digitized SPRI-NSF-TUD bed picks data are available through the BAS
195 webpage (<https://data.bas.ac.uk/metadata.php?id=GB/NERC/BAS/AEDC/00326>). The two-dimensional SAR-processed
196 radargrams in SEG-Y format for the IMAFI survey are provided at doi.org/10.5285/8a975b9e-f18c-4c51-9bdb-b00b82da52b8,
197 whereas the ice thickness datasets in Comma Separated Value (CSV) format for both GRADES/IMAGE and IMAFI are
198 available via the BAS aerogeophysical processing portal (<https://secure.antarctica.ac.uk/data/aerogeo/>). The ice thickness data
199 for IMAFI are provided in two folders; (1) the region of thinner ice (200m) picked from the pulse dataset and (2) the overall
200 ice thickness data, derived from picking of SAR-processed CHIRP radargrams. The data are arranged according to the latitude,
201 longitude, ice thickness values and the pulse repetition interval (PRI) radar shot number which is used to index the raw data.
202 The OIB SAR images (Level 1B) in MAT (binary MATLAB) format and the radar depth sounder Level 2 (L2) data in CSV
203 format are available via the CReSIS website (<https://data.cresis.ku.edu/>). The L2 data include measurements for GPS time
204 during data collection, latitude, longitude, elevation, surface, bottom and thickness. For more information on these data, the
205 reader should refer to the appropriate CReSIS data information and guidance notes for each field season (i.e.
206 https://data.cresis.ku.edu/data/rds/rds_readme.pdf).

207

208 4.1 GRADES/IMAGE and Institute-Möller Antarctic Funding Initiative data processing

209

210 The waveform was retrieved and sequenced according to its respective transmit pulse type. The modified data were then
211 collated using Matlab standard format. Doppler filtering (Hélière et al., 2007) was used to remove the backscattering hyperbola
212 in the along-track direction (Corr et al., 2007; Ross et al., 2012). Chirp compression was then applied to the along-track data.
213 Unfocused synthetic aperture (SAR) processing was used for the GRADES/IMAGE survey by applying a moving average of
214 33 data points (Corr et al., 2007) whereas 2D-SAR (i.e. focused) processing based on Omega-K algorithm was used to process
215 the IMAFI data (Hélière et al., 2007; Winter et al., 2015) to enhance both along-track resolution and echo signal noise. The
216 bed echo was depicted in a semi-automatic manner using PROMAX seismic processing software. All picking for IMAFI was
217 undertaken by a single operator (Neil Ross). A nominal value of 10 m is used to correct for the firn layer during the processing
218 of ice thickness, which introduces an error of the order of $\pm 3 \text{ m}$ across the survey field (Ross et al., 2012). This is small relative
219 to the total error budget of the order of $\pm 1\%$. Finally, the GPS and RES data were combined to determine the ice thickness,
220 ice-surface and bed elevation datasets. Elevations are measured with reference to WGS84. The ice surface elevation was



221 calculated by subtracting terrain clearance from the height of the aircraft, whereas the bed elevation was computed by
222 subtracting the ice thickness from the ice surface elevation.

223

224 4.2 OIB data processing

225

226 The OIB radar adopts SAR processing in the along-track direction to provide higher resolution images of the subglacial profile.
227 The data were processed in three steps to improve the signal-to-noise ratio and increase the along-track resolution (Gogineni
228 et al., 2014). The raw data were first converted from a digital quantization level to a receiver voltage level. The surface was
229 captured using the low-gain data, microwave radar or laser altimeter. A normalized matched filter with frequency-domain
230 windowing was then used for pulse compression. 2D-SAR processing was used after conditioning the data, which is based on
231 the frequency-wavenumber (F-K) algorithm. The F-K SAR processing, however, requires a straight and uniformly sampled
232 data which are usually not met in the raw data since the aircraft's speed is not consistent and the trajectory is not straight. The
233 raw data were thus spatially resampled in along-track using sinc kernel to approximate a uniformly sampled dataset. The
234 vertical deviation in aircraft trajectory from the horizontal flight path was compensated in the frequency domain with a time-
235 delay phase shift. The phase shift was later removed for array processing as it is able to account for the non-uniform sampling;
236 the purpose is to maintain the original geometry for the array processing. Array processing was performed in the cross-track
237 flightpath to reduce surface clutter as well as improving the signal-to-noise ratio. Both the delay-and-sum and Minimum
238 Variance Distortionless Response (MVDR) beamformer were used to combine the multichannel data, and for regions with
239 significant surface clutter the MVDR beamformer could effectively minimize the clutter power and pass the desired signal
240 with optimum weights (Harry and Trees, 2002).

241

242 4.3 Quantifying ice thickness, bed topography and subglacial water flow

243

244 The new ice thickness DEM was formed from all the available RES data using the 'Topo to Raster' function in ArcGIS, based
245 on the Australian National University Digital Elevation Model (ANUDEM) elevation gridding algorithm (Hutchinson, 1988).
246 The ice thickness picks from the geophysical data were gridded using the Nearest Neighbour interpolation within Topo to
247 Raster. The ice thickness DEM was then subtracted from the ice-sheet surface elevation derived from the combined European
248 Remote Sensing Satellite-1 (ERS-1) radar and Ice, Cloud and land Elevation Satellite (ICESat) laser satellite altimetry DEM
249 (Bamber et al., 2009a), to derive the bed topography. The ice thickness, ice-sheet surface and bed elevations were then gridded
250 at a uniform 1 km spacing, and referenced to the Polar Stereographic projection (Snyder, 1987) to form the new DEMs. The
251 difference map between the new DEM and the Bedmap2 product (Fretwell et al., 2013) was computed by subtracting the
252 Bedmap2 bed elevation DEM from the new bed elevation DEM. Crossover analysis for the 2006/7 data onwards (including
253 data acquired on flightlines beyond the extent of our DEM) shows the RMS errors of 9.1 m (GRADES/IMAGE), 15.82 m
254 (IMAFI), 45.93 m (CRESIS 2012), 23.74 m (CRESIS 2014) and 20.27 m (CRESIS 2016).

255 Subglacial water flowpaths were calculated based on the hydraulic potentiometric surface principle, in which basal water
256 pressure is balanced by the ice overburden pressure as follows:

257

$$258 \varphi = (\rho_w \times g \times y) + (\rho_i \times g \times h) \quad (1)$$

259

260 where φ is the theoretical hydropotential surface, y is the bed elevation, h is the ice thickness, ρ_w and ρ_i are the density of
261 water (1000 kg m^{-3}) and ice (920 kg m^{-3}), assuming ice to be homogenous, respectively, and g is the gravitational constant
262 (9.81 ms^{-2}) (Shreve, 1972). Sinks in the hydrostatic pressure field raster were filled to produce realistic hydrologic flowpaths.
263 The 'flow direction' of the raster was then defined by assigning each cell a direction to the steepest downslope neighbouring
264 cell. Sub-basins less than 200 km^2 were removed due to the coarse input of bed topography and ice thickness DEMs.

265

266 5. Results

267

268 5.1 A new 1-km digital elevation model of the Weddell Sea sector

269

270 We present a new DEM of the WS sector of West Antarctica, compiled from several airborne geophysical radar surveys (Fig.
271 3a). The Bedmap2 bed elevation and the difference map are shown in Fig. 3b and 3c respectively. The new DEM contains
272 substantial changes in certain regions, whereas in others there are consistencies between the two DEMs, for example across
273 the Bungenstock ice rise, where there are little new data. The mean error between the two DEMs is -86.45 m indicating a
274 slightly lower bed elevation in the new DEM data compared to Bedmap2, which is likely the result of deep parts of the
275 topography (i.e. valley bottoms) not being visible in the fieldwork non-SAR processed QC radargrams for the IMAFI project
276 (e.g. Horsehoe Valley, near Patriot Hills in the Ellsworth Mountains (Winter, 2016). The bed elevation measurement upstream



277 of the Bungenstock ice rise and across the Robin Subglacial Basin shows a generally good agreement with Bedmap2; only
278 some portions of new DEM across the Möller ice stream, Pagano Shear zone and Pirrit Hills area are significantly different
279 from Bedmap2, with differences in bed elevation typically ranging between -109 m to 172 m (Fig. 3c). There is, however,
280 large disagreement between the two DEMs in the western region of Institute ice stream, across the Ellsworth Mountains (e.g.
281 in the Horseshoe valley), the Foundation ice stream and towards East Antarctica where topography is more rugged. It is also
282 worth noting the significant depth of the bed topography beneath the trunk of the Foundation ice stream, where a trough more
283 than ~2 km deep is located and delineated (Fig. 3d). The trough is ~38 km wide and ~80 km in length, with the deepest section
284 ~2.3 km below sea level. The new DEM shows a significant change in the depiction of Foundation Trough; we have measured
285 it to be ~1 km deeper relative to the Bedmap2 product.

286 In order to further quantify the differences between Bedmap2 and our new DEM, we present terrain profiles of both
287 DEMs relative to four RES flightlines (Fig. 3c). It is worth noting that the new DEM is much more consistent with the bed
288 elevations from the RES data picks compared to Bedmap2 (Fig. 4a and 4b). The new DEM show a correlation coefficient of
289 0.96 and 0.91 for Profile A and B, respectively. This is slightly higher compared with the Bedmap2 which is 0.94 (Profile A)
290 and 0.91 (Profile B). Although inaccuracies of the bed elevation persist across the Foundation ice stream for both DEMs, the
291 gross pattern of the bed elevation for the new DEM is much more consistent with the RES transect relative to the Bedmap2
292 (Fig. 4c and 4d) with correlation coefficient of 0.97 and 0.94 for Profile C and D, respectively. In contrast, the correlation
293 coefficient for the profile produced by Bedmap2 (0.87 for Profile C and 0.82 for Profile D) are significantly reduced.

294

295 5.2 Hydrology

296

297 Computing the potential passageway of subglacial water beneath the ice-sheet is critical for comprehending ice-sheet dynamics
298 (Bell, 2008; Stearns et al., 2008; Siegert et al., 2016a). It is noted that the development of subglacial hydrology pathways is
299 highly sensitive to ice-surface elevation, and to a lesser degree by bed morphology (Wright et al., 2008; Horgan et al., 2013).
300 Figure 3d shows a comparison of subglacial hydrology pathways between our new bed DEM and the Bedmap2 DEM. The
301 gross patterns of water flow are largely unchanged between the two DEMs, especially across and upstream of Institute and
302 Möller ice stream. The similar water pathway pattern between both DEMs in these regions is also consistent with the small
303 error in bed topography (Fig. 3c). Despite large differences in bed topography across the Foundation ice stream and the
304 Ellsworth Mountains region, the large-scale patterns of water flow are also similar between both DEMs; this is due to the
305 dominance of the ice-surface slope in driving basal water flow in these regions (Shreve, 1972). Nonetheless, there are several
306 local small-scale differences in the water pathways (Fig. 3d), which highlight hydraulic sensitivity. The subglacial water
307 network observed in the new DEM across the Foundation ice stream appears to be more arborescent than that derived from
308 Bedmap2. This is due to the introduction of new data, resulting in a better-defined bed across the Foundation Trough (Fig. 3d).
309 It is also worth noting that the pattern of the subglacial water pathway observed in the new DEM adjacent to the grounding
310 line across the Möller ice stream is almost in good agreement with the position of sub-ice-shelf channels, which have been
311 delineated from a combination of satellite images and RES data (Le Brocq et al., 2013).

312 Subglacial lakes discovered across the WS sector form a vital constituent of the basal hydrological system (Wright and
313 Siegert, 2012). These lakes exist due to sufficient amount of geothermal heating ($50 \text{ mW m}^{-2} - 70 \text{ mW m}^{-2}$) which melts the
314 base of the ice sheet. In addition, the pressure exerted by the overlying ice causes the melting point of the ice to be lowered.
315 At the western margin of the Ellsworth Mountain lies a large body of the subglacial water known as Ellsworth Subglacial Lake
316 ($-78^\circ 59' 24''\text{N}$, $269^\circ 25' 48''\text{E}$). The lake measures 28.9 km^2 with a depth ranging between 52 m to 156 m capable of carrying
317 a water body volume of 1.37 km^3 (Woodward et al., 2010). There are 4 known subglacial lakes distributed across the Institute
318 ice stream (Wright and Siegert, 2012). The Institute W1 ($-81^\circ 24' 3.6''\text{N}$, $282^\circ 27' 18''\text{E}$) is located close to the Robin Subglacial
319 Basin A whereas Institute W2 ($-81^\circ 37' 40.8''\text{N}$, $276^\circ 25' 15.6''\text{E}$) is located to the northeast of Pirrit Hill. The Institute E1 ($-$
320 $82^\circ 7' 48''\text{N}$, $285^\circ 30' 32.4''\text{E}$) and E2 ($-82^\circ 37' 30''\text{N}$, $280^\circ 59' 13.2''\text{E}$) are located to the southwest of Robin Subglacial Basin
321 B and near the field camp of C110, respectively. In addition, there are three subglacial lakes in the Foundation ice stream
322 catchment: Foundation 1 ($-84^\circ 31' 19.2''\text{N}$, $286^\circ 20' 16.8''\text{E}$); Foundation 2 ($-84^\circ 59' 2.4''\text{N}$, $286^\circ 1' 44.4''\text{E}$); and Foundation 3
323 ($-85^\circ 15' 28.8''\text{N}$, $287^\circ 12' 25.2''\text{E}$) (Wright and Siegert, 2012).

324

325 5.3 Geomorphological description of the bed topography

326

327 The WS sector of WAIS is composed of three major ice-sheet outlets (Fig. 1a); the Institute, Möller and Foundation ice streams,
328 feeding ice to the FRIS, the second largest ice shelf in Antarctica after the Ross Ice Shelf. Recent geophysical inspection of
329 the subglacial topography in the region reveals features such as steep reverse bed slopes, similar in scale to that measured for
330 upstream Thwaites Glacier, close to the Institute and Möller ice stream grounding lines. The bed slopes inland to a ~1.8 km
331 deep basin (the Robin Subglacial Basin), which is divided into two sections, with few obvious significant ice-sheet pinning
332 points (Ross et al., 2012). Elevated beds in other parts of the WS sector allow the ice shelf to ground, causing ice surface



333 features known as ice rises and rumpled (Matsuoka et al., 2015). The Bungenstock ice rise (Siegert et al., 2013) is excellent
334 example of an ice rise, though peculiarly is an ice rise that is grounded far below sea level.

335 The Institute ice stream has three tributaries, within our survey grid, to the south and west of the Ellsworth Mountains,
336 occupying the Horseshoe Valley, Independence and Ellsworth troughs (Fig. 1b) (Winter et al., 2015). The Horseshoe Valley
337 Trough, around 20 km wide and 1.3 km below sea level at its deepest point, is located downstream of the steep mountains of
338 the Heritage Range. A subglacial ridge is located between the mouth of the Horseshoe Valley Trough and the main trunk of
339 the Institute ice stream (Winter et al., 2015). The Independence Trough is located subparallel to the Horseshoe Valley Trough,
340 separated by the 1.4 km high of the Independence Hills. The trough is ~22 km wide and is 1.1 km below sea level at its deepest
341 point. It is characterized by two distinctive plateaus (~6 km wide each) on each side of the trough, aligned alongside the main
342 trough axis. Ice flows eastward through the Independence Trough for ~54 km before it shifts to a northward direction where
343 the trough widens to 50 km and its connection with the main Institute ice stream. The Ellsworth Trough is aligned with the
344 Independence Trough, and both are orthogonal to the orientation of the Amundsen – Weddell ice divide, dissecting the
345 Ellsworth Subglacial Highlands northwest to southeast. The Ellsworth Trough measures ~34 km in width and is ~2 km below
346 sea level at its deepest point, and is ~260 km in length. It is considered to be the largest and deepest trough-controlled tributary
347 in this region (Winter et al., 2015). The Ellsworth Trough is intersected by several smaller valleys aligned perpendicularly to
348 the main axis, which are relics landforms from a previous small dynamic ice mass (predating the WAIS in its present
349 configuration) (Ross et al., 2014). The Ellsworth Trough contains ~15 – 20 km long Ellsworth Subglacial Lake (Siegert et al.,
350 2004a; Woodward et al., 2010; Siegert et al., 2012; Wright and Siegert, 2012).

351 Satellite altimetry and imagery are able to estimate the grounding line that separates the grounded ice sheet from the
352 floating ice shelf, based on surface changes due to tidal oscillations and the subtle ice surface features. Such analysis is prone
353 to uncertainty, however. There are currently four proposed grounding line locations, based on different satellite data sets and/or
354 methods of analysis (Bohlander and Scambos, 2007; Bindschadler et al., 2011; Brunt et al., 2011; Rignot et al., 2011a). Each
355 of the grounding lines were delineated from satellite images, but without direct measurement of the subglacial environment.
356 This results in ambiguities in the precise location of the transition between floating and grounded ice (Jeofry et al., 2017). In
357 addition, RES data have demonstrated clear errors in the position of the grounding line with a large, hitherto unknown,
358 subglacial embayment near the Institute ice stream grounding line. The subglacial embayment is ~1 km deep and is potentially
359 open to the ice shelf cavity, causing the inland ice sheet to have a direct contact with ocean water. In addition, our RES analysis
360 reveals a better- defined Foundation Trough, in which the grounding line is perched on very deep topography around 2 km
361 below sea level.

362 A previous study revealed a series of ancient large sub-parallel subglacial bed channels between MIS and FIS, adjacent
363 to the Marginal Basins (Fig. 1b) (Rose et al., 2014). While these subglacial channels are likely to have been formed by the
364 flow of basal water, they are presently located beneath slow moving and cold-based ice. It is thought, therefore, that the
365 channels are ancient and were formed at a time when surface melting was prevalent in West Antarctica (e.g. the Pliocene).

366 The bed topography of the WS appears both rough (over the mountains and exposed bedrock) and smooth (across the
367 sediment-filled regions) (Bingham and Siegert, 2007). Although there is no specific method or standardized unit to measure
368 bed roughness, studies of bed roughness calculated using Fast Fourier Transform (FFT) technique based on the relative
369 measurement of bed obstacle amplitude and frequency of the roughness obstacles have indicated that the IIS and MIS are
370 dominated by relatively low roughness values, less than 0.1 (Bingham and Siegert, 2007; Rippin et al., 2014), which was
371 suggested as being the result of the emplacement of marine sediments as in the Siple Coast region (Siegert et al., 2004b; Peters
372 et al., 2005). Radar-derived roughness analysis has evidenced a smooth bed across the Robin Subglacial Basin where sediments
373 may exist (Rippin et al., 2014). The deepest parts of the Robin Subglacial Basin are anomalously rough, marking the edge of
374 a sedimentary drape where the highest ice flow velocities are generated (Siegert et al., 2016b). As such, the smooth basal
375 topography of the Institute and Möller ice stream catchments is less extensive than proposed by Bingham and Siegert (2007).
376 It has been demonstrated since, that the subglacial topography of the region between the Robin Subglacial Basin and the Pirrit
377 and Martin-Nash Hills is relatively flat, smooth and gently sloping, and has been interpreted as a bedrock planation surface
378 (Rose et al., 2015). This zone of the study area was originally interpreted by Bingham and Siegert (2009) as underlain by fine-
379 grained marine sediments, due to the limited RES data available to them at the time. Although the exact formation process of
380 the planation surface is unknown, it is thought that this geomorphological feature formed due to marine and/or fluvial erosion
381 (Rose et al., 2015).

382

383 6. Data availability

384

385 The new 1 km bed elevation product of the Weddell Sea sector, West Antarctica can be found in the <http://doi.org/10.5281/zeno>
386 [do.1035488](https://doi.org/10.5281/zeno). We used four radar datasets to construct the 1 km ice thickness DEM, as follows: (1) Digitized radar data from
387 the 1970s SPRI-NSF-TUD surveys, in which the bed was picked every 15-20 seconds (1-2 km), recorded here in an Excel 97-
388 2003 Worksheet (XLS), which can be obtained from the UK Polar Data Centre (UKPDC) website at



389 <https://data.bas.ac.uk/metadata.php?id=GB/NERC/BAS/AEDC/00326>; (2) BAS GRADES/IMAGE and (3) BAS IMAFI
390 airborne surveys, both available from the UKPDC Polar Airborne Geophysics Data Portal at <https://secure.antarctica.ac.uk/data/aerogeo/>; and (4) NASA Operation IceBridge radar depth sounder Level 2 (L2) data, available from the Center for Remote
391 Sensing of Ice Sheet (CRISIS) website at <https://data.cresis.ku.edu/>.
392

393
394 The 1 km ice-sheet surface elevation DEM was derived from a combination of ERS-1 surface radar and ICESat laser altimetry,
395 which is downloadable from the National Snow and Ice Data Center (NSIDC) website at https://nsidc.org/data/docs/daac/nsidc_0422_antarctic_1km_dem/.
396

397
398 Two-dimensional SAR-processed radargrams in SEG-Y format for the BAS IMAFI airborne survey, and The NASA Operation
399 IceBridge SAR images (Level 1B) in MAT (binary MATLAB) format, are provided at doi.org/10.5285/8a975b9e-f18c-4c519bdb-b00b82da52b8 and <https://data.cresis.ku.edu/>, respectively.
400

401
402 Ancillary information for the MEASURES InSAR-based ice velocity map of Central Antarctica can be found at
403 [doi:10.5067/MEASURES/CRYOSPHERE/nsidc-0484.001](https://doi.org/10.5067/MEASURES/CRYOSPHERE/nsidc-0484.001) and the MODIS Mosaic of Antarctica 2008 – 2009 (MOA2009)
404 ice sheet surface image map is available at doi.org/10.7265/N5KP8037. The RADARSAT (25m) ice-sheet surface satellite
405 imagery is accessible from the Byrd Polar and Climate Research Center website at <http://research.bpcrc.osu.edu/rsl/radarsat/data/>.
406

407
408 A summary of the data used in this paper, and their availability is provided in the table 1.
409

410 7. Conclusions

411
412 We have compiled airborne radar data from a number of geophysical surveys, including the SPRI-NSF-TUD surveys of the
413 1970s, the GRADES/IMAGE and IMAFI surveys acquired by BAS in 2006/7 and 2010/11, respectively, and new geophysical
414 datasets collected by the CRISIS from the NASA OIB project in 2012, 2014 and 2016. From these data, we produce a bed
415 topography DEM with high spatial resolution (1km). The DEM covers a total area of ~125,000 km² of the Weddell Sea sector
416 including the Institute ice stream, Bungenstock ice rise, Möller and Foundation ice streams. Large differences can be observed
417 between the new DEM and that of the previous DEM of the region (Bedmap2), most notably across the Foundation ice stream,
418 where we reveal the grounding line to be resting on a bed ~2 km below sea level, with a deep trough immediately upstream as
419 deep as 2.3 km below sea level. In addition, the bed elevation of our DEM appears to be slightly lower relative to the bed
420 elevation of Bedmap2 DEM, which is likely the results of the deep sections of the topography not being visible in the fieldwork
421 non-SAR processed radargrams. Our new DEM also revises the pattern of potential basal water flow across the Foundation
422 ice stream and towards East Antarctica in comparison to that derived from Bedmap2. Our new DEM, and the data used to
423 compile it, is available to download, and will be of value to ice-sheet modelling experiments in which the accuracy of the DEM
424 is important to ice flow processes in this particularly sensitive region of the WAIS.

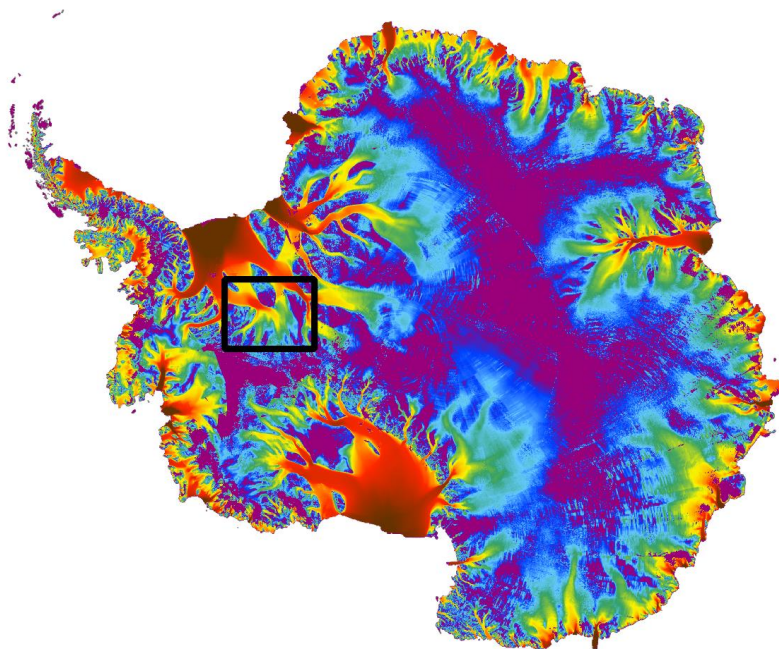
425
426 **Author contributions.** Hafeez Jeofry carried out the analysis, created the figures, wrote the paper and compiled the database.
427 All authors contributed to the database compilation, analysis and writing of the paper.
428

429 **Competing interests.** The authors declare that they have no conflict of interest.
430

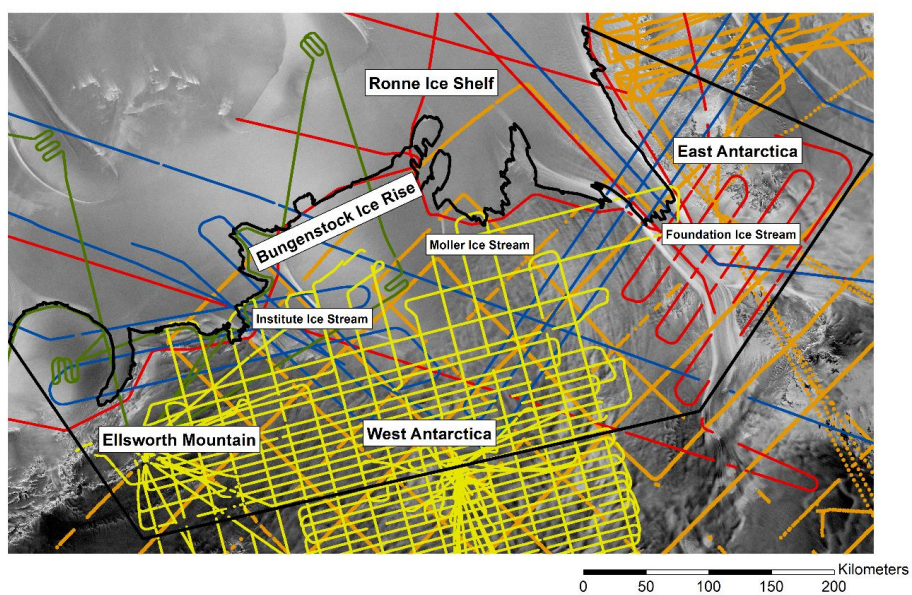
431 **Acknowledgement.** The data used in this project are available at the Center for the Remote Sensing of Ice data portal
432 <https://data.cresis.ku.edu/> and at the UK Airborne Geophysics Data Portal <https://secure.antarctica.ac.uk/data/aerogeo/>.
433 Prasad Gogineni and Jilu Li acknowledge funding by NASA for CRISIS data collection and development of radars
434 (NNX10AT68G), Martin J. Siegert, Neil Ross, Hugh F.J. Corr, Fausto Ferraccioli, Rob Bingham, Anne Le Brocq, David
435 Rippin, Tom Jordan, Carl Robinson, Doug Cochrane, Ian Potten and Mark Oostlander acknowledge funding from the NERC
436 Antarctic Funding Initiative (NE/G013071/1) and Hafeez Jeofry acknowledges funding from the Ministry of Higher Education
437 Malaysia and the Norwegian Polar Institute for the Quantarctica GIS package.



a.



b.





c.

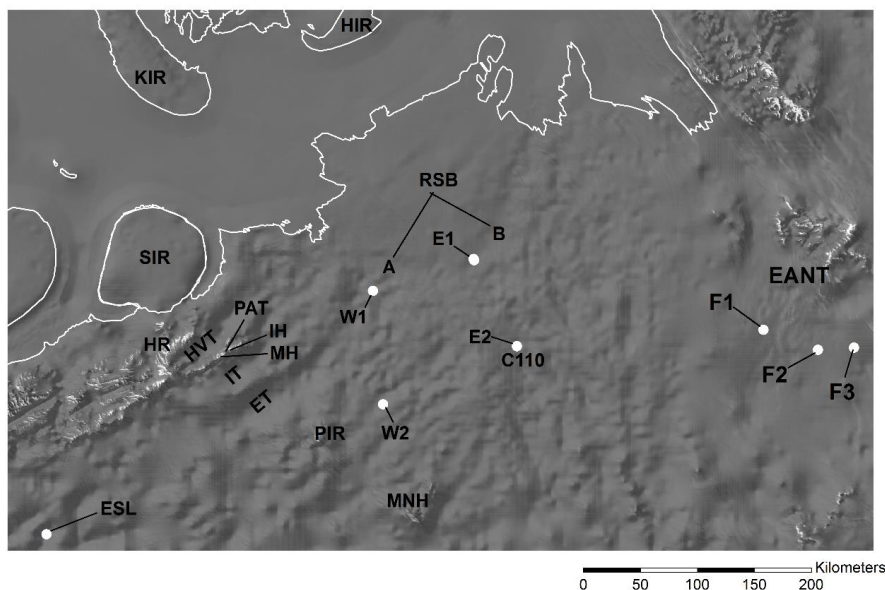
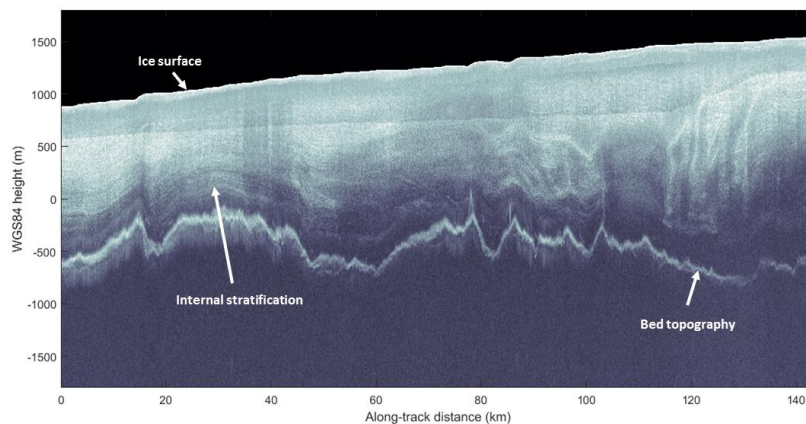


Figure 1. Map of: (a) A location inset of Antarctica overlain with InSAR-derived ice surface velocities (Rignot et al., 2011b); (b) The aerogeophysical flight lines across Weddell Sea sector superimposed over RADARSAT (25m) satellite imagery mosaic (Jezek, 2002); SPRI airborne survey 1969 – 1979 (orange); BAS GRADES/IMAGE survey 2008 (green); BAS Institute ice stream survey 2010/2011 (IMAFI) (yellow); OIB 2012 (red); and OIB 2014 (blue); (c) Map of the Weddell Sea sector on MODIS imagery (Haran et al., 2014); Annotations: KIR – Korff ice rise; HIR – Henry ice rise; SIR – Skytrain ice rise; HR – Heritage Range; HVT – Horseshoe Valley Trough; IT – Independence Trough; ET – Ellsworth Trough; ESL – Ellsworth Subglacial Lake; E1 – Institute E1 Subglacial Lake; E2 – Institute E2 Subglacial Lake; W1 – Institute W1 Subglacial Lake; W2 Institute W2 Subglacial Lake; F1 – Foundation 1 Subglacial Lake; F2 – Foundation 2 Subglacial Lake; F3 – Foundation 3 Subglacial Lake; PAT – Patriot Hills; IH – Independence Hills; MH – Marble Hills; PIR – Pirrit Hills; MNH – Martin-Nash Hills; RSB – Robin Subglacial Basin; and EANT – East Antarctica.



a.



b.

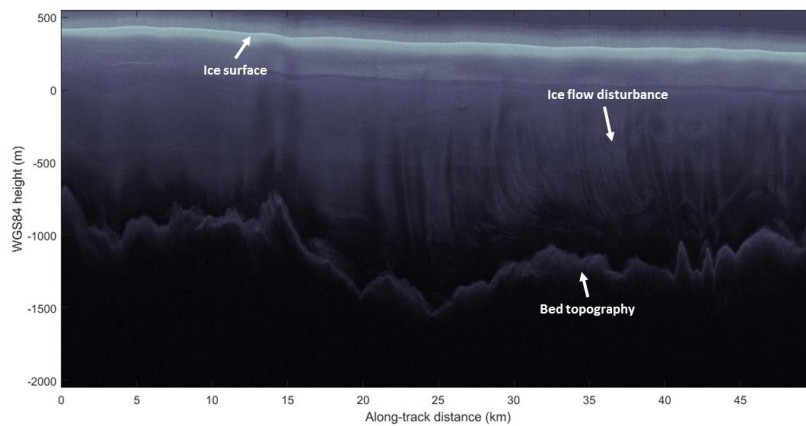
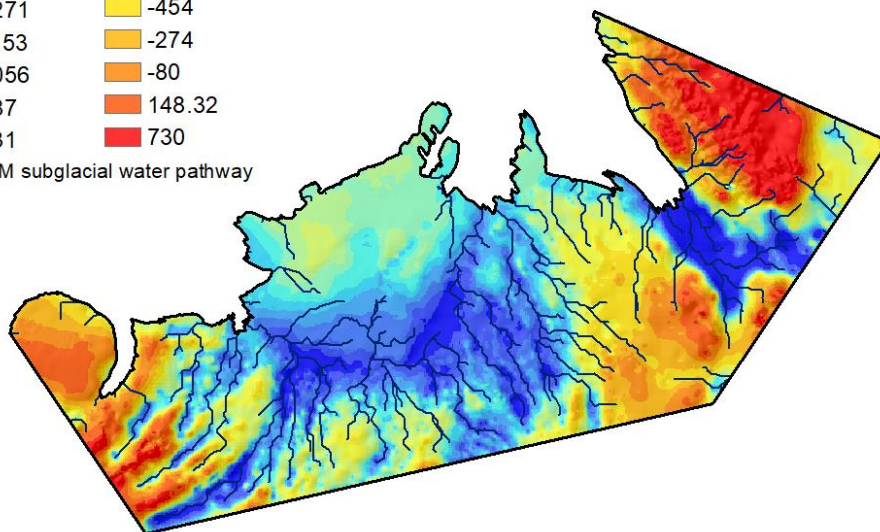
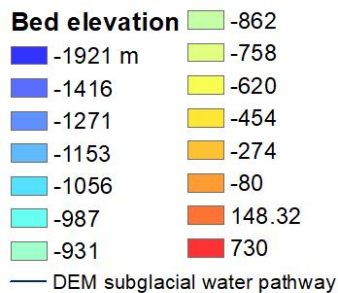


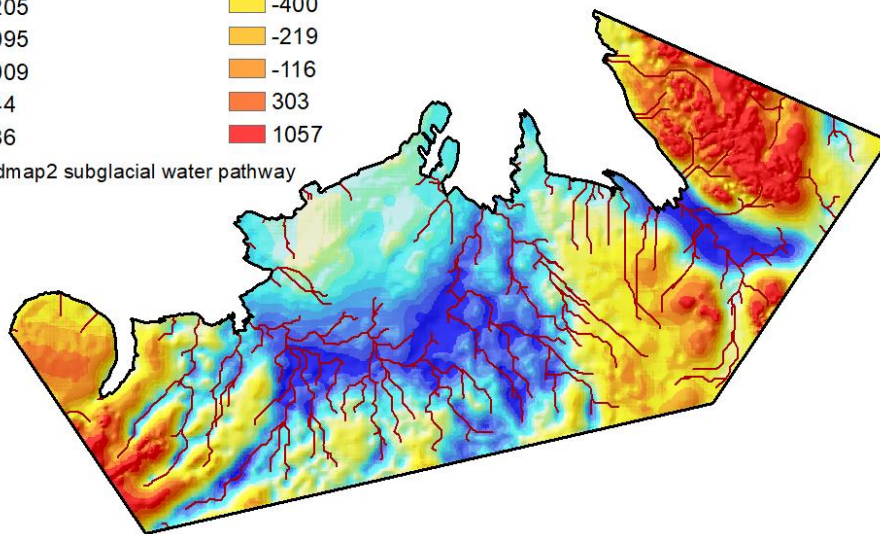
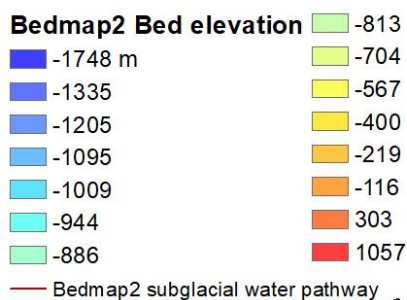
Figure 2. Two-dimensional synthetic aperture radar (SAR) processed radargrams of: (a) BAS IMAFI data (b) OIB data.



a.

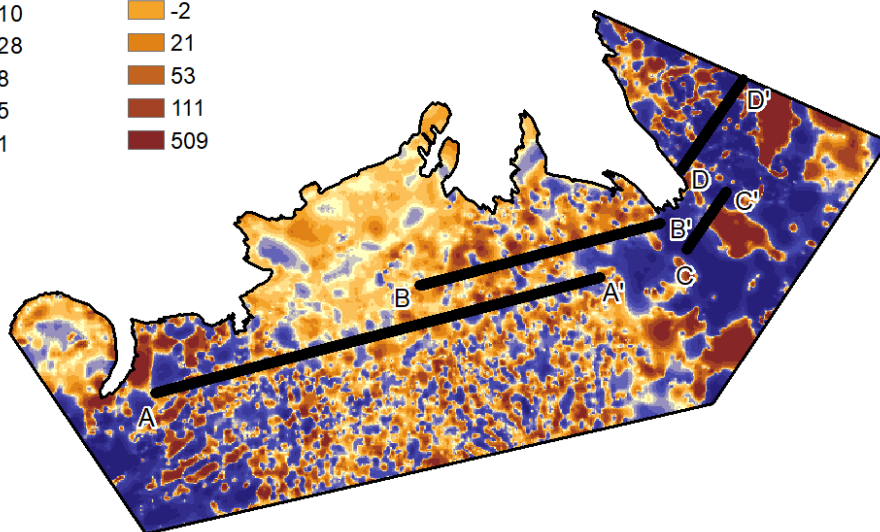
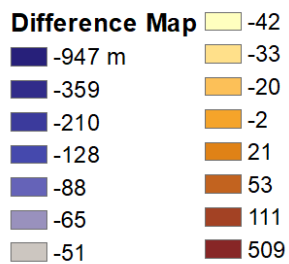


b.





c.



d.

— Bedmap2 subglacial water pathway
— DEM subglacial water pathway

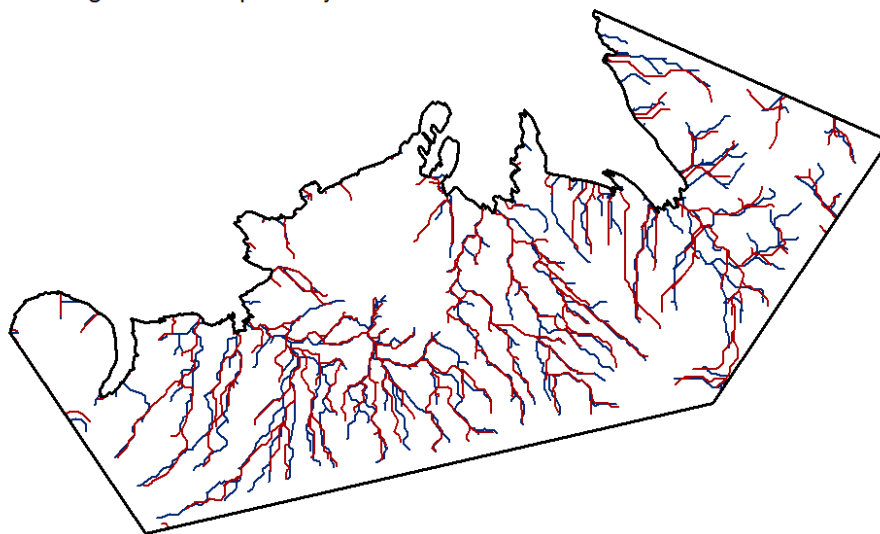
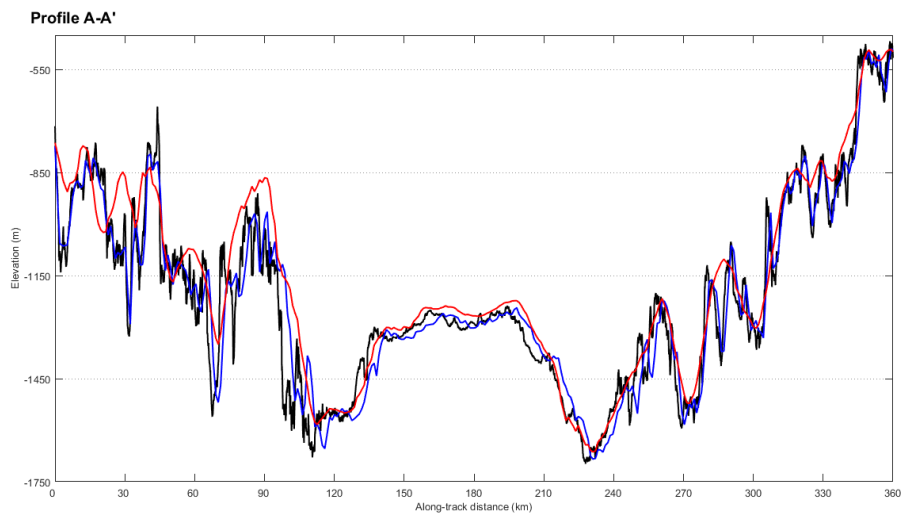




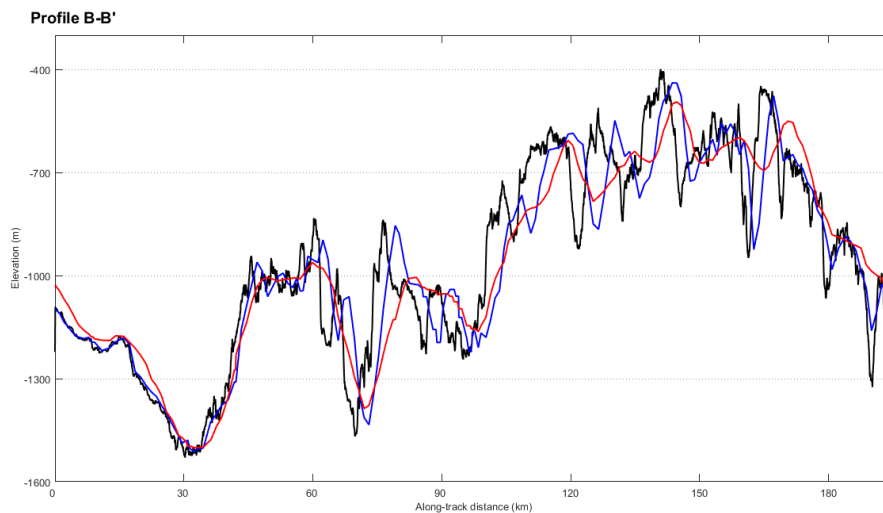
Figure 3. Map of: (a) A new bed topography digital elevation model; (b) Bedmap2 bed elevation product (Fretwell et al., 2013); (c) Profile A – A', B – B', C – C' and D – D' overlain by error map showing differences in bed elevation between the new DEM and Bedmap2; and (d) DEM and Bedmap2 subglacial water pathway.



a.

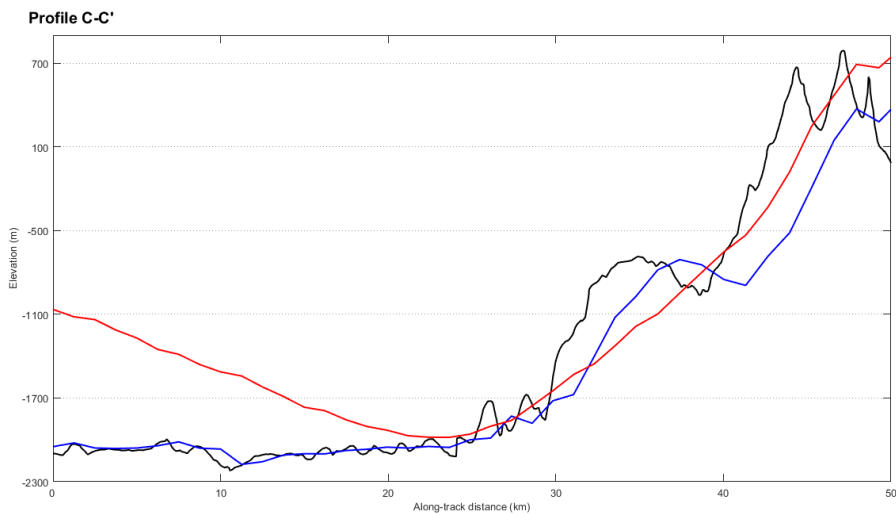


b.





c.



d.

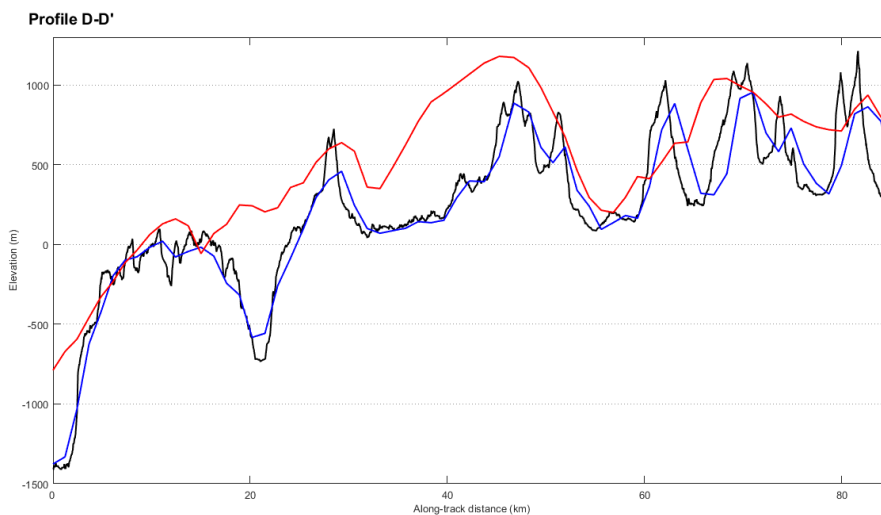


Figure 4. Bed elevation for the RES transect (black), DEM (blue) and Bedmap2 (red) of: (a) Profile A – A’; (b) Profile B – B’; (c) Profile C – C’; and (d) Profile D – D’.

**Table 1:** Data files and locations.

Products	Files	Location	DOI/URL
1-km bed elevation DEM	1-km bed elevation DEM	Zenodo Data Repository	http://doi.org/10.5281/zenodo.1035488
1-km ice thickness DEM	Digitized SPRI-NSF-TUD bed picks data	UK Polar Data Centre (UKPDC)	https://data.bas.ac.uk/metadata.php?id=GB/NERC/BAS/AEDC/00326
	BAS GRADES/IMAGE ice thickness data	UK Polar Data Centre (UKPDC)	https://secure.antarctica.ac.uk/data/aerogeo/
	BAS IMAFI ice thickness data	UK Polar Data Centre (UKPDC)	https://secure.antarctica.ac.uk/data/aerogeo/
	NASA Operation IceBridge radar depth sounder Level 2 (L2) data	Center for Remote Sensing of Ice Sheet (CReSIS)	https://data.cresis.ku.edu/
1-km ice sheet surface DEM	ERS-1 radar and ICESat laser satellite altimetry	National Snow and Ice Data Center (NSIDC)	https://nsidc.org/data/docs/daac/nsidc0422_antarctic_1km_dem/
Two-dimensional synthetic aperture radar (SAR) processed radargrams	BAS IMAFI airborne survey	UK Polar Data Centre (UKPDC)	doi.org/10.5285/8a975b9e-f18c-4c51-9bdb-b00b82da52b8
	NASA Operation IceBridge airborne survey	Center for Remote Sensing of Ice Sheet (CReSIS)	https://data.cresis.ku.edu/
Ice velocity map of Central Antarctica	MEASUREs InSAR-based ice velocity	National Snow and Ice Data Center (NSIDC)	doi:10.5067/MEASURES/CRYOSPHERE/nsidc-0484.001
Ice sheet surface satellite imagery	MODIS Mosaic of Antarctica (2008 – 2009) (MOA2009)	National Snow and Ice Data Center (NSIDC)	doi.org/10.7265/N5KP8037
	RADARSAT (25m) satellite imagery	Byrd Polar and Climate Research Center	http://research.bpcrc.osu.edu/rsl/radarsat/data/



References

- 438 Ashmore, D. W., Bingham, R. G., Hindmarsh, R. C., Corr, H. F., and Joughin, I. R.: The relationship between sticky
439 spots and radar reflectivity beneath an active West Antarctic ice stream, *Annals of Glaciology*, 55, 29-38, 2014.
- 440 Bamber, J., Gomez-Dans, J., and Griggs, J.: Antarctic 1 km digital elevation model (DEM) from combined ERS-1
441 radar and ICESat laser satellite altimetry, National Snow and Ice Data Center, Boulder, 2009a. 2009a.
- 442 Bamber, J. L., Riva, R. E., Vermeersen, B. L., and LeBrocq, A. M.: Reassessment of the potential sea-level rise
443 from a collapse of the West Antarctic Ice Sheet, *Science*, 324, 901-903, 2009b.
- 444 Bell, R. E.: The role of subglacial water in ice-sheet mass balance, *Nature Geoscience*, 1, 297-304, 2008.
- 445 Bindschadler, R., Choi, H., and Collaborators, A.: High-resolution image-derived grounding and hydrostatic lines
446 for the Antarctic Ice Sheet, Digital media, National Snow and Ice Data Center, Boulder, Colorado, USA, 2011.
447 2011.
- 448 Bingham, R. G. and Siegert, M. J.: Quantifying subglacial bed roughness in Antarctica: implications for ice-sheet
449 dynamics and history, *Quaternary Science Reviews*, 28, 223-236, 2009.
- 450 Bingham, R. G. and Siegert, M. J.: Radar-derived bed roughness characterization of Institute and Möller ice
451 streams, West Antarctica, and comparison with Siple Coast ice streams, *Geophysical Research Letters*, 34, 2007.
- 452 Bohlander, J. and Scambos, T.: Antarctic coastlines and grounding line derived from MODIS Mosaic of Antarctica
453 (MOA), National Snow and Ice Data Center, Boulder, CO, USA, 2007. 2007.
- 454 Brunt, K. M., Fricker, H. A., and Padman, L.: Analysis of ice plains of the Filchner–Ronne Ice Shelf, Antarctica,
455 using ICESat laser altimetry, *Journal of Glaciology*, 57, 965-975, 2011.
- 456 Budd, W., Jenssen, D., and Smith, I.: A three-dimensional time-dependent model of the West Antarctic ice
457 sheet, *Annals of Glaciology*, 5, 29-36, 1984.
- 458 Christensen, E. L.: Radioglaciology 300 MHz radar, Technical University [of] Denmark, Electromagnetics
459 Institute, 1970.
- 460 Corr, H. F., Ferraccioli, F., Frearson, N., Jordan, T., Robinson, C., Armadillo, E., Caneva, G., Bozzo, E., and
461 Tabacco, I.: Airborne radio-echo sounding of the Wilkes Subglacial Basin, the Transantarctic Mountains and the
462 Dome C region, *Terra Antarctica Reports*, 13, 55-63, 2007.
- 463 Dowdeswell, J. A. and Evans, S.: Investigations of the form and flow of ice sheets and glaciers using radio-echo
464 sounding, *Reports on Progress in Physics*, 67, 1821, 2004.
- 465 Drewry, D. and Meldrum, D.: Antarctic airborne radio echo sounding, 1977–78, *Polar Record*, 19, 267-273, 1978.
- 466 Drewry, D., Meldrum, D., and Jankowski, E.: Radio echo and magnetic sounding of the Antarctic ice sheet, 1978–
467 79, *Polar Record*, 20, 43-51, 1980.
- 468 Drewry, D. J.: Antarctica, Glaciological and Geophysical Folio, University of Cambridge, Scott Polar Research
469 Institute, 1983.
- 470 Fretwell, P., Pritchard, H. D., Vaughan, D. G., Bamber, J. L., Barrand, N. E., Bell, R., Bianchi, C., Bingham, R. G.,
471 Blankenship, D. D., Casassa, G., Catania, G., Callens, D., Conway, H., Cook, A. J., Corr, H. F. J., Damaske, D.,
472 Damm, V., Ferraccioli, F., Forsberg, R., Fujita, S., Gim, Y., Gogineni, P., Griggs, J. A., Hindmarsh, R. C. A.,
473 Holmlund, P., Holt, J. W., Jacobel, R. W., Jenkins, A., Jokat, W., Jordan, T., King, E. C., Kohler, J., Krabill, W., Riger-
474 Kusk, M., Langley, K. A., Leitchenkov, G., Leuschen, C., Luyendyk, B. P., Matsuoka, K., Mouginot, J., Nitsche, F. O.,
475 Nogi, Y., Nost, O. A., Popov, S. V., Rignot, E., Rippin, D. M., Rivera, A., Roberts, J., Ross, N., Siegert, M. J., Smith,
476 A. M., Steinhage, D., Studinger, M., Sun, B., Tinto, B. K., Welch, B. C., Wilson, D., Young, D. A., Xiangbin, C., and
477 Zirizzotti, A.: Bedmap2: improved ice bed, surface and thickness datasets for Antarctica, *The Cryosphere*, 7, 375-
478 393, 2013.
- 479 Gogineni, P.: CRESeS Radar Depth Sounder Data, Lawrence, Kansas, USA, Digital Media,
480 <http://data.cresis.ku.edu/>, 2012. 2012.
- 481 Gogineni, S., Yan, J.-B., Paden, J., Leuschen, C., Li, J., Rodriguez-Morales, F., Braaten, D., Purdon, K., Wang, Z.,
482 and Liu, W.: Bed topography of Jakobshavn Isbræ, Greenland, and Byrd Glacier, Antarctica, *Journal of*
483 *Glaciology*, 60, 813-833, 2014.
- 484 Graham, F. S., Roberts, J. L., Galton-Fenzi, B. K., Young, D., Blankenship, D., and Siegert, M. J.: A high-resolution
485 synthetic bed elevation grid of the Antarctic continent, *Earth System Science Data Discussions*, doi:
486 10.5194/essd-2016-18, 2016. 1-18, 2016.
- 487 Haran, T., Bohlander, J., Scambos, T., Painter, T., and Fahnestock, M.: MODIS Mosaic of Antarctica 2008–2009
488 (MOA2009) Image Map, Boulder, Colorado USA: National Snow and Ice Data Center, doi, 10, N5KP8037, 2014.
- 489 Harry, L. and Trees, V.: Optimum array processing: part IV of detection, estimation, and modulation theory, John
490 Wiley and Sons, Inc, 2002. 2002.



- 491 Hélière, F., Lin, C.-C., Corr, H., and Vaughan, D.: Radio echo sounding of Pine Island Glacier, West Antarctica:
492 Aperture synthesis processing and analysis of feasibility from space, *IEEE Transactions on Geoscience and*
493 *Remote Sensing*, 45, 2573-2582, 2007.
- 494 Hellmer, H. H., Kauker, F., Timmermann, R., Determann, J., and Rae, J.: Twenty-first-century warming of a large
495 Antarctic ice-shelf cavity by a redirected coastal current, *Nature*, 485, 225-228, 2012.
- 496 Horgan, H. J., Alley, R. B., Christianson, K., Jacobel, R. W., Anandakrishnan, S., Muto, A., Beem, L. H., and
497 Siegfried, M. R.: Estuaries beneath ice sheets, *Geology*, 41, 1159-1162, 2013.
- 498 Hutchinson, M. F.: Calculation of hydrologically sound digital elevation models, August 17-19 1988, 117-133,
499 1988.
- 500 Jacobs, S. S., Jenkins, A., Giulivi, C. F., and Dutrieux, P.: Stronger ocean circulation and increased melting under
501 Pine Island Glacier ice shelf, *Nature Geoscience*, 4, 519-523, 2011.
- 502 Jankowski, E. J. and Drewry, D.: The structure of West Antarctica from geophysical studies, *Nature*, 291, 17-21,
503 1981.
- 504 Jeofry, H., Ross, N., Corr, H. F., Li, J., Gogineni, P., and Siegert, M. J.: A deep subglacial embayment adjacent to
505 the grounding line of Institute Ice Stream, West Antarctica, Geological Society, London, Special Publications,
506 461, SP461. 411, 2017.
- 507 Jezek, K. C.: RADARSAT-1 Antarctic Mapping Project: change-detection and surface velocity campaign, *Annals of*
508 *Glaciology*, 34, 263-268, 2002.
- 509 Jordan, T. A., Ferraccioli, F., Ross, N., Corr, H. F. J., Leat, P. T., Bingham, R. G., Rippin, D. M., le Brocq, A., and
510 Siegert, M. J.: Inland extent of the Weddell Sea Rift imaged by new aerogeophysical data, *Tectonophysics*, 585,
511 137-160, 2013.
- 512 Kennicutt, M., Kim, Y., Rogan-Finnemore, M., Anandakrishnan, S., Chown, S. L., Colwell, S., Cowan, D., Escutia,
513 C., Frenot, Y., and Hall, J.: Delivering 21st century Antarctic and Southern Ocean science, *Antarctic Science*, 28,
514 407-423, 2016.
- 515 Kennicutt, M. C., Chown, S. L., Cassano, J. J., Liggett, D., Massom, R., Peck, L. S., Rintoul, S. R., Storey, J. W. V.,
516 Vaughan, D. G., Wilson, T. J., and Sutherland, W. J.: Polar Research: Six priorities for Antarctic science, *Nature*,
517 512, 23-25, 2014.
- 518 Le Brocq, A. M., Payne, A. J., and Vieli, A.: An improved Antarctic dataset for high resolution numerical ice sheet
519 models (ALBMAP v1), *Earth System Science Data*, 2, 247-260, 2010.
- 520 Le Brocq, A. M., Ross, N., Griggs, J. A., Bingham, R. G., Corr, H. F., Ferraccioli, F., Jenkins, A., Jordan, T. A., Payne,
521 A. J., and Rippin, D. M.: Evidence from ice shelves for channelized meltwater flow beneath the Antarctic Ice
522 Sheet, *Nature Geoscience*, 6, 945-948, 2013.
- 523 Lindbäck, K., Pettersson, R., Doyle, S. H., Helanow, C., Jansson, P., Kristensen, S. S., Stenseng, L., Forsberg, R.,
524 and Hubbard, A. L.: High-resolution ice thickness and bed topography of a land-terminating section of the
525 Greenland Ice Sheet, *Earth System Science Data*, 6, 331-338, 2014.
- 526 Lythe, M. B. and Vaughan, D. G.: BEDMAP: A new ice thickness and subglacial topographic model of Antarctica,
527 *Journal of Geophysical Research: Solid Earth*, 106, 11335-11351, 2001.
- 528 Martin, M. A., Levermann, A., and Winkelmann, R.: Comparing ice discharge through West Antarctic Gateways:
529 Weddell vs. Amundsen Sea warming, *The Cryosphere Discussions*, 9, 1705-1733, 2015.
- 530 Matsuoka, K., Hindmarsh, R. C. A., Moholdt, G., Bentley, M. J., Pritchard, H. D., Brown, J., Conway, H., Drews, R.,
531 Durand, G., Goldberg, D., Hattermann, T., Kingslake, J., Lenaerts, J. T. M., Martín, C., Mulvaney, R., Nicholls, K.
532 W., Pattyn, F., Ross, N., Scambos, T., and Whitehouse, P. L.: Antarctic ice rises and rumples: Their properties and
533 significance for ice-sheet dynamics and evolution, *Earth-Science Reviews*, 150, 724-745, 2015.
- 534 Peters, M. E., Blankenship, D. D., and Morse, D. L.: Analysis techniques for coherent airborne radar sounding:
535 Application to West Antarctic ice streams, *Journal of Geophysical Research: Solid Earth*, 110, 2005.
- 536 Pritchard, H. D.: Bedgap: where next for Antarctic subglacial mapping?, *Antarctic Science*, 26, 742, 2014.
- 537 Rignot, E., Mouginot, J., and Scheuchl, B.: MEaSURES Antarctic Grounding Line from Differential Satellite Radar
538 Interferometry, National Snow and Ice Data Center: Boulder, CO, USA, 2011a. 2011a.
- 539 Rignot, E., Mouginot, J., and Scheuchl, B.: MEaSURES InSAR-based Antarctica ice velocity map, National Snow
540 and Ice Data Center: Boulder, CO, USA, 2011b. 2011b.
- 541 Rippin, D., Bingham, R., Jordan, T., Wright, A., Ross, N., Corr, H., Ferraccioli, F., Le Brocq, A., Rose, K., and
542 Siegert, M.: Basal roughness of the Institute and Möller Ice Streams, West Antarctica: Process determination
543 and landscape interpretation, *Geomorphology*, 214, 139-147, 2014.
- 544 Ritz, C., Edwards, T. L., Durand, G., Payne, A. J., Peyaud, V., and Hindmarsh, R. C.: Potential sea-level rise from
545 Antarctic ice-sheet instability constrained by observations, *Nature*, 528, 115-118, 2015.



- 546 Rodriguez-Morales, F., Gogineni, S., Leuschen, C. J., Paden, J. D., Li, J., Lewis, C. C., Panzer, B., Alvestegui, D. G.-
547 G., Patel, A., and Byers, K.: Advanced multifrequency radar instrumentation for polar research, *IEEE*
548 *Transactions on Geoscience and Remote Sensing*, 52, 2824-2842, 2014.
- 549 Rose, K. C., Ross, N., Bingham, R. G., Corr, H. F. J., Ferraccioli, F., Jordan, T. A., Le Brocq, A. M., Rippin, D. M., and
550 Siegert, M. J.: A temperate former West Antarctic ice sheet suggested by an extensive zone of subglacial
551 meltwater channels, *Geology*, 42, 971-974, 2014.
- 552 Rose, K. C., Ross, N., Jordan, T. A., Bingham, R. G., Corr, H. F., Ferraccioli, F., Le Brocq, A. M., Rippin, D. M., and
553 Siegert, M. J.: Ancient pre-glacial erosion surfaces preserved beneath the West Antarctic Ice Sheet, *Earth*
554 *Surface Dynamics*, 3, 139, 2015.
- 555 Ross, N., Bingham, R. G., Corr, H. F. J., Ferraccioli, F., Jordan, T. A., Le Brocq, A., Rippin, D. M., Young, D.,
556 Blankenship, D. D., and Siegert, M. J.: Steep reverse bed slope at the grounding line of the Weddell Sea sector in
557 West Antarctica, *Nature Geoscience*, 5, 393-396, 2012.
- 558 Ross, N., Jordan, T. A., Bingham, R. G., Corr, H. F., Ferraccioli, F., Le Brocq, A., Rippin, D. M., Wright, A. P., and
559 Siegert, M. J.: The Ellsworth subglacial highlands: inception and retreat of the West Antarctic Ice Sheet,
560 *Geological Society of America Bulletin*, 126, 3-15, 2014.
- 561 Shi, L., Allen, C. T., Ledford, J. R., Rodriguez-Morales, F., Blake, W. A., Panzer, B. G., Prokopiack, S. C., Leuschen,
562 C. J., and Gogineni, S.: Multichannel coherent radar depth sounder for NASA operation ice bridge, 2010, 1729-
563 1732.
- 564 Shreve, R.: Movement of water in glaciers, *Journal of Glaciology*, 11, 205-214, 1972.
- 565 Siegert, M., Ross, N., Corr, H., Kingslake, J., and Hindmarsh, R.: Late Holocene ice-flow reconfiguration in the
566 Weddell Sea sector of West Antarctica, *Quaternary Science Reviews*, 78, 98-107, 2013.
- 567 Siegert, M. J.: On the origin, nature and uses of Antarctic ice-sheet radio-echo layering, *Progress in Physical*
568 *Geography*, 23, 159-179, 1999.
- 569 Siegert, M. J., Clarke, R. J., Mowlem, M., Ross, N., Hill, C. S., Tait, A., Hodgson, D., Parnell, J., Tranter, M., and
570 Pearce, D.: Clean access, measurement, and sampling of Ellsworth Subglacial Lake: a method for exploring deep
571 Antarctic subglacial lake environments, *Reviews of Geophysics*, 50, 2012.
- 572 Siegert, M. J., Hindmarsh, R., Corr, H., Smith, A., Woodward, J., King, E. C., Payne, A. J., and Joughin, I.: Subglacial
573 Lake Ellsworth: A candidate for in situ exploration in West Antarctica, *Geophysical Research Letters*, 31, 2004a.
- 574 Siegert, M. J., Ross, N., Corr, H., Smith, B., Jordan, T., Bingham, R., Ferraccioli, F., Rippin, D., and Le Brocq, A.:
575 Boundary conditions of an active West Antarctic subglacial lake: implications for storage of water beneath the
576 ice sheet, 2014. 2014.
- 577 Siegert, M. J., Ross, N., and Le Brocq, A. M.: Recent advances in understanding Antarctic subglacial lakes and
578 hydrology, *Phil. Trans. R. Soc. A*, 374, 20140306, 2016a.
- 579 Siegert, M. J., Ross, N., Li, J., Schroeder, D. M., Rippin, D., Ashmore, D., Bingham, R., and Gogineni, P.: Subglacial
580 controls on the flow of Institute Ice Stream, West Antarctica, *Annals of Glaciology*, 2016b. 1-6, 2016b.
- 581 Siegert, M. J., Taylor, J., Payne, A. J., and Hubbard, B.: Macro-scale bed roughness of the siplé coast ice streams
582 in West Antarctica, *Earth Surface Processes and Landforms*, 29, 1591-1596, 2004b.
- 583 Skou, N. and Søndergaard, F.: Radioglaciology. A 60 MHz ice sounder system, Technical University of Denmark,
584 1976.
- 585 Snyder, J. P.: Map projections--A working manual, US Government Printing Office, Washington, D.C., 1987.
- 586 Stearns, L. A., Smith, B. E., and Hamilton, G. S.: Increased flow speed on a large East Antarctic outlet glacier
587 caused by subglacial floods, *Nature Geoscience*, 1, 827-831, 2008.
- 588 Stocker, T.: Climate change 2013: the physical science basis: Working Group I contribution to the Fifth
589 assessment report of the Intergovernmental Panel on Climate Change, Cambridge University Press, 2014.
- 590 Thoma, M., Determann, J., Grosfeld, K., Goeller, S., and Hellmer, H. H.: Future sea-level rise due to projected
591 ocean warming beneath the Filchner Ronne Ice Shelf: A coupled model study, *Earth and Planetary Science*
592 *Letters*, 431, 217-224, 2015.
- 593 Winter, K.: Englacial stratigraphy, debris entrainment and ice sheet stability of Horseshoe Valley, West
594 Antarctica, 2016. Doctoral thesis, University of Northumbria, Newcastle upon Tyne, England, UK, 263 pp., 2016.
- 595 Winter, K., Woodward, J., Ross, N., Dunning, S. A., Bingham, R. G., Corr, H. F. J., and Siegert, M. J.: Airborne
596 radar evidence for tributary flow switching in Institute Ice Stream, West Antarctica: Implications for ice sheet
597 configuration and dynamics, *Journal of Geophysical Research: Earth Surface*, 120, 1611-1625, 2015.
- 598 Woodward, J., Smith, A. M., Ross, N., Thoma, M., Corr, H., King, E. C., King, M., Grosfeld, K., Tranter, M., and
599 Siegert, M.: Location for direct access to subglacial Lake Ellsworth: An assessment of geophysical data and
600 modeling, *Geophysical Research Letters*, 37, 2010.



- 601 Wright, A. and Siegert, M.: A fourth inventory of Antarctic subglacial lakes, *Antarctic Science*, 24, 659-664, 2012.
602 Wright, A., Siegert, M., Le Brocq, A., and Gore, D.: High sensitivity of subglacial hydrological pathways in
603 Antarctica to small ice-sheet changes, *Geophysical Research Letters*, 35, 2008.
604 Wright, A. P., Le Brocq, A. M., Cornford, S. L., Bingham, R. G., Corr, H. F. J., Ferraccioli, F., Jordan, T. A., Payne, A.
605 J., Rippin, D. M., Ross, N., and Siegert, M. J.: Sensitivity of the Weddell Sea sector ice streams to sub-shelf
606 melting and surface accumulation, *The Cryosphere*, 8, 2119-2134, 2014.